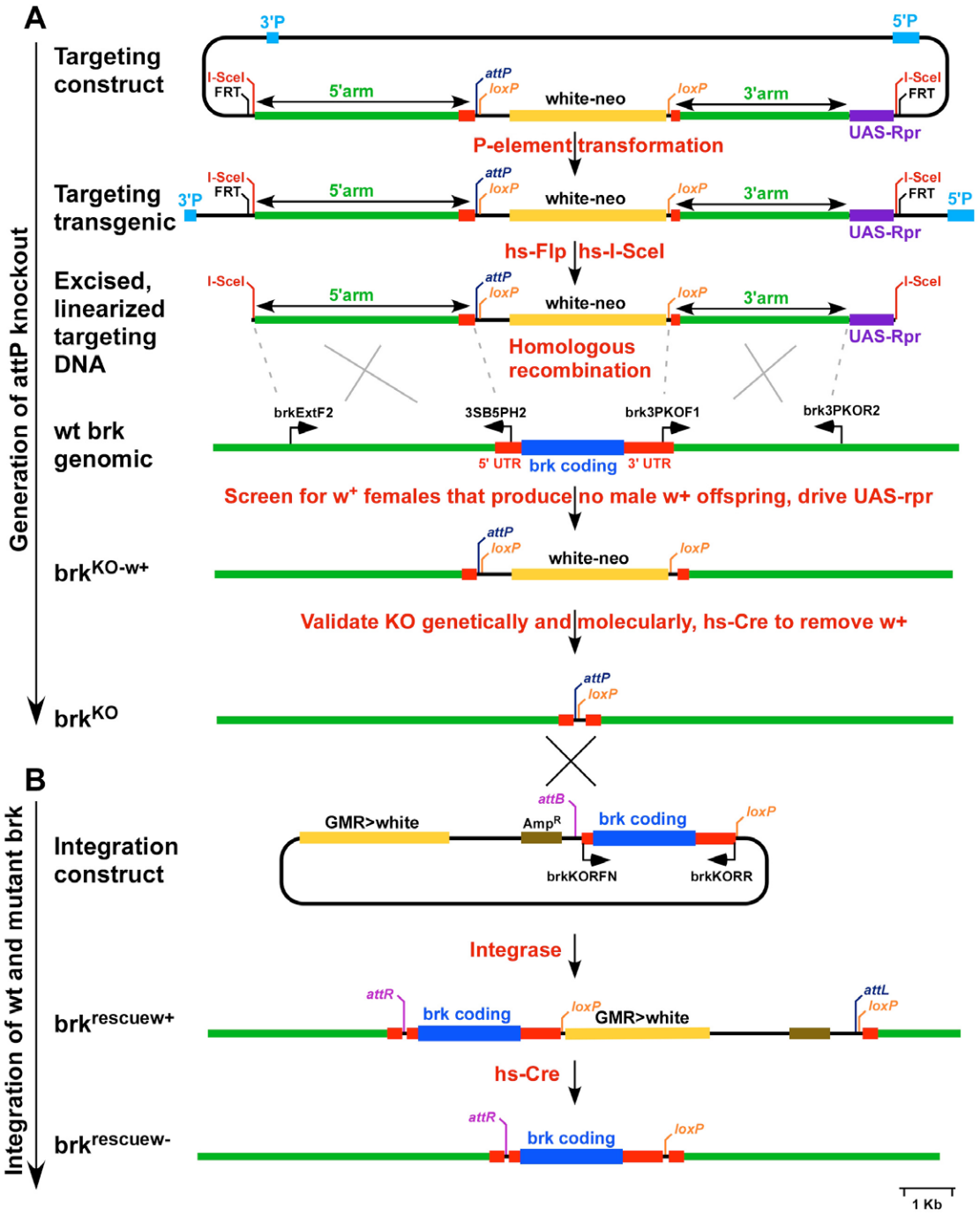


**Fig. S1. Generation of endogenous *brk* mutants.** This was achieved using the procedures of Golic and Hong and co-workers (Rong and Golic, 2000; Gong and Golic, 2003; Huang et al., 2008; Huang et al., 2009; Zhou et al, 2012) (A) Generation of *brk* knockout ($brk^{KO}$) by a modified ends out gene targeting approach. A targeting construct was made in vector pGX-PCM1 (this is identical to the pGX-attP-WN vector (Zhou et al, 2012) with the absence of the SphI site) comprising: (i) 5' and 3' *brk* flanking regions/arms extending into the 5' and 3' UTRs (primers for PCR to generate these arms is shown in Fig. S2 and Table S1), (ii) a ØC31 bacteriophage *attP* site positioned 3' to the 5' *brk* arm, (iii) *white* (*w*+) marker flanked by *loxP* sites, positioned between the *brk* arms (iv) UAS-rpr outside of the region containing the arms, to select against non-targeted events, (v) FRT and I-Sce-I sites that flank elements i-iv, and (vi) P-element ends for integration into the genome of *w*- flies. Following P-element mediated-transgenesis, Flippase and I-Sce-I were used to excise and linearize targeting DNA in vivo. Non-targeted events were selected against by crossing to Gal4221[w-] to drive UAS-rpr (which will make such events lethal). 15,000 progeny were screened for *w*+ females (*brk* is on the X) not carrying the original targeting transgene yielding six hundred potential candidates. Out of these ten failed to produce $w^+$ males and all were characterized as brk KOs molecularly and genetically (Fig. S2, 3) and finally the *w*+ marker was excised using Cre, resulting in the final $brk^{KO}$ in which the *brk* gene is replaced by an *attP* site and *loxP* site.
(B) Integration of wild-type and mutant forms of *brk* into the *attP* site of $brk^{KO}$. Integration constructs were made consisting of a *brk* gene extending from the regions in the 5' and 3' UTRs not included in the arms used in the targeting construct, the *brk* gene is flanked 5' by an *attB* site and 3' by a *loxP* site, and a *w*+ marker. This is integrated into $brk^{KO}$ using ØC31 integrase and the *w*+ marker is excised from the resulting transformants using Cre resulting in a fly carrying a *brk* gene that is identical to the wild-type with the exception of an *attR* site and *loxP* site in the 5' and 3' UTRs, respectively, along with any modification made to *brk*.

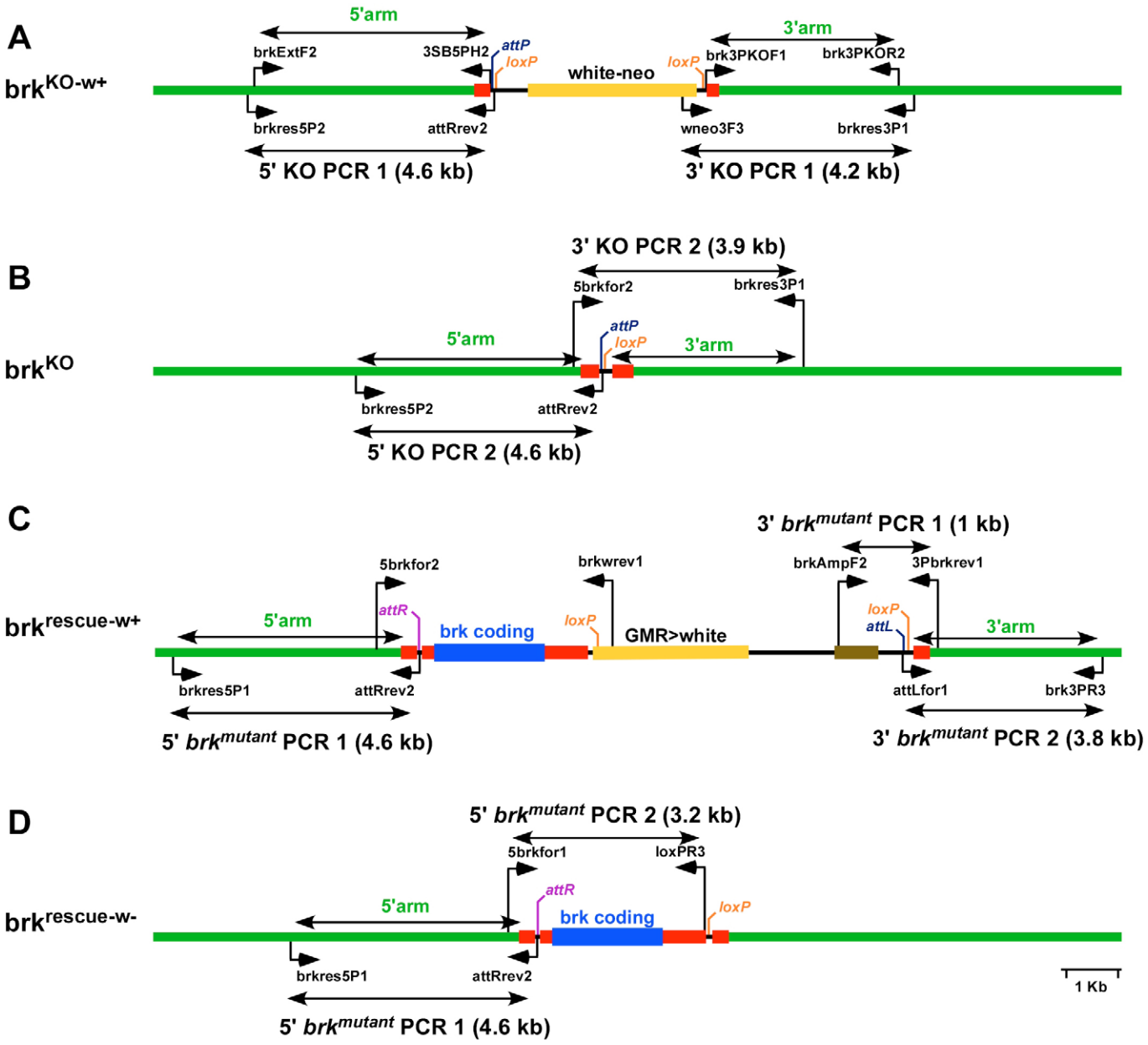


**Fig. S2. Molecular validation of *brk*$^{KO}$ and endogenous *brk* mutants.** All genotypes indicated were confirmed by PCR amplification of genomic DNA including the novel 5' and 3' ends created by the procedures (expected amplicon size indicated), followed by restriction mapping and sequencing. The PCR was performed with primers outside of those used to generate the arms used in the targeting construct. Validation of the final mutant was also confirmed by amplifying the *brk* gene using a primer in the region including the novel *loxP* sequence in the 3' UTR and a 5' primer outside of the transcription unit. Sequences of primers are listed in Table S1.


**Fig. S3. Genetic validation of *brk*$^{KO}$ and restoration of function in *brk*$^{rescue}$.** (A-D) Adult wings. (A) Wild-type with longitudinal veins indicated, L2-L5. (B) The *brk*$^{XGXM2}$ hypomorph has a slightly enlarged posterior, incomplete L5 and a fused alula (arrowed). *brk*$^{XGXM2}$ is a previously unpublished viable allele generated by mobilisation of a P-element insertion, *brk*$^{XG}$ (Campbell, unpublished). (C) The *brk*$^{XGXM2}$ phenotypes are more severe over a null allele, *brk*$^{F124}$. (D) The *brk*$^{XGXM2}$/*brk*$^{KO}$ is comparable in severity to the null over *brk*$^{XGXM2}$. (E) Functional validation of *brk*$^{rescue}$. The viability of *brk*$^{rescue}$ heterozygotes over a series of embryonic lethal *brk* mutants, *brk*$^{M68}$, *brk*$^{F124}$, *brk*$^{F138}$, *brk*$^{E427}$, a *brk* deficiency and the larval/pupal lethal *brk*$^{XA}$ was calculated and compared to heterozygotes of a wild-type allele over the same mutants. Although the average is slightly reduced for *brk*$^{rescue}$ heterozygotes, the difference with the wild-type heterozygotes was not significant (n = 3, in each experiment at least 100 females were evaluated, P > 0.05, Mann Whitney U test) indicating that the integration of a wild-type *brk* allele at the deletion locus in the *brk*$^{KO}$ restores and rescues the native *brk* locus functionally.

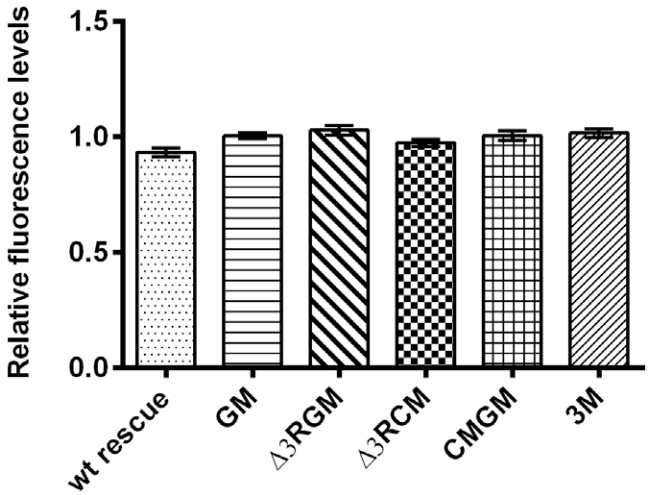


**Fig. S4. Comparison of mutant Brk protein levels to wild-type.** Wing discs carrying clones of the genotypes indicated were stained with Brk antibody, imaged on a confocal taking care the detector was not saturated and, using ImageJ, the average fluorescence level within a clone situated in the lateral region was compared to the average within an adjacent wild-type twin spot, a value of 1 will then indicate no difference. For every *brk* mutant, twenty independently generated clones were assessed and the average fluorescence level within a clone was measured along with the average within an adjacent wild-type twin spot and the relative difference was calculated; a relative value of 1 will then indicate no difference and a Chi-square test with trend was used to determine whether relative mutant Brk/wild-type levels were significantly different from this 'expected' value. As shown in the scatter-plot the twenty mutant Brk fluorescence values relative to wild-type for every *brk* mutant do not differ significantly from the expected wild-type value of 1, indicated with red dashed line (P > 0.05, chi-square test for trend).

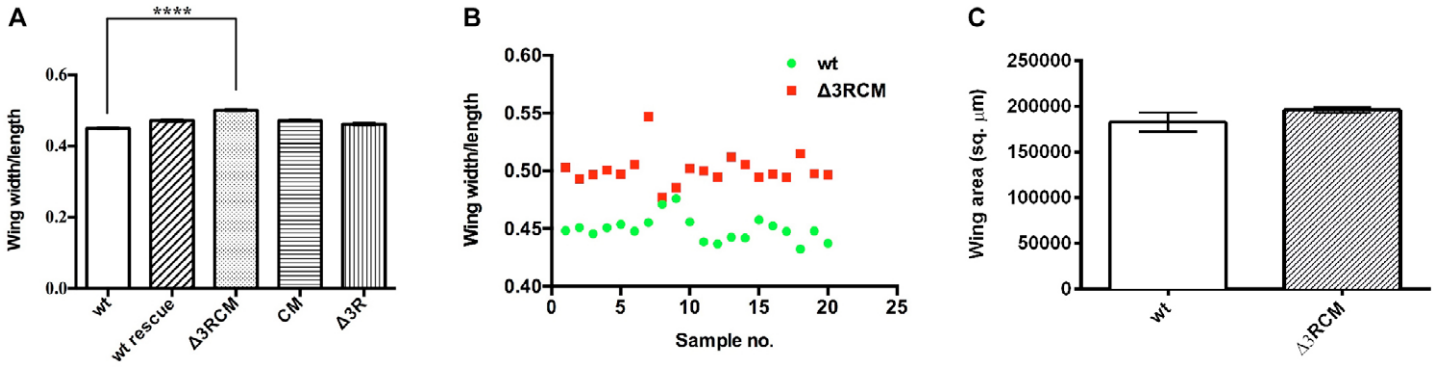


**Fig. S5 Comparison of adult wing size in wild-type to that of viable *brk* mutants.** (A,B) Ratio of width to length. This ratio for $brk^{\Delta 3RCM}$ wings is slightly, but significantly, higher than wild-type (n = 20, P < 0.0001, Mann Whitney U test) while that of $brk^{rescue}$, $brk^{CM}$, $brk^{\Delta 3R}$ is not (n = 10 for each mutant, P > 0.05, Kruskal Wallis test followed by Dunn's multiple comparison). (B) Scatter-plot of the width/length ratios of $brk^{\Delta 3RCM}$ and wild-type wings showing that for a few $brk^{\Delta 3RCM}$ wings the width/length ratio approaches close to the wild-type but is increased for most. (C) The area of $brk^{\Delta 3RCM}$ wings does not vary significantly from the wild-type (n = 20 for each genotype, P > 0.05, Mann Whitney U test).

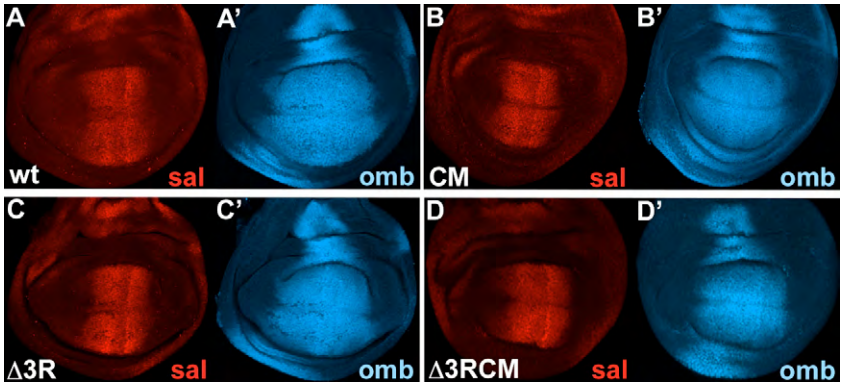


**Fig. S6. *sal* and *omb* expression in viable *brk* mutants.** Third instar wing discs stained for omb-lacZ (ß-gal antibody) and Sal (antibody), anterior left. Expression of *sal* and ombZ in $brk^{CM}$, $brk^{\Delta 3R}$, $brk^{\Delta 3RCM}$ (B-D) is indistinguishable from that in the wild-type (A).

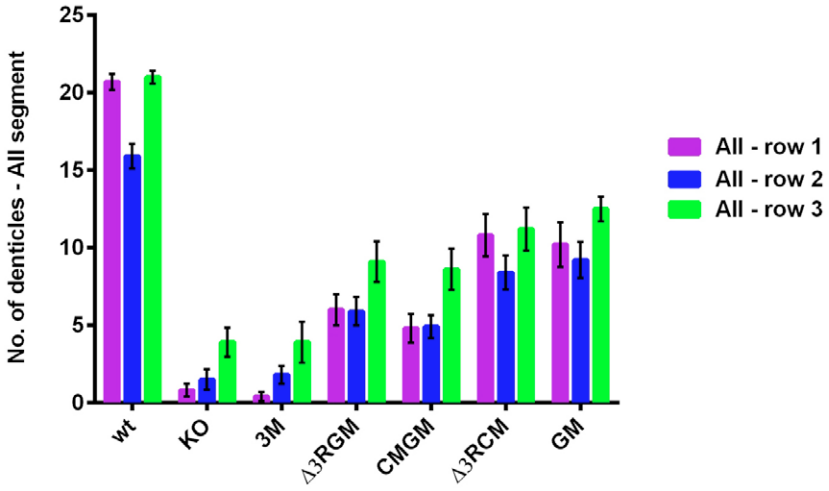


**Fig. S7. Comparison of the number of denticles in rows 1-3 of the VDB of the second abdominal segment (AII) in wild-type and *brk* mutants**. Number of denticles remaining in rows 1-3 of AII ventral denticle belt are in significantly reduced in the following *brk* mutants, $brk^{KO}$, $brk^{3M}$, $brk^{\Delta 3RGM}$, $brk^{CMGM}$, $brk^{\Delta 3RCM}$ and $brk^{GM}$ (n = 10, P < 0.01, Mann Whitney U test). The loss of denticles is most severe in $brk^{KO}$ and $brk^{3M}$, of intermediate severity in $brk^{\Delta 3RGM}$ and $brk^{CMGM}$ and milder in $brk^{GM}$ and $brk^{\Delta 3RCM}$. All mutants except $brk^{\Delta 3RCM}$ display a polarity defect, such that all the remaining denticles point posteriorly compared to the wild-type where denticles in rows 1 and 4 point anteriorly while rest point posteriorly.

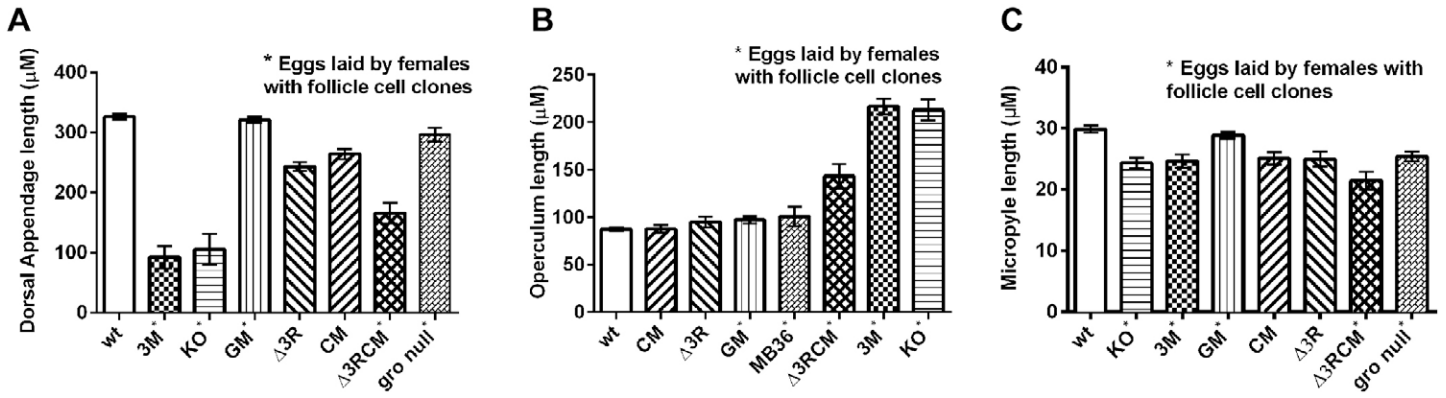


**Fig. S8. Size of the dorsal appendages (DAs), operculum and micropyle in eggs laid by mutant mothers or mothers carrying follicle cell clones.** Eggs laid by mothers with follicle cell clones are marked with * Compared to wild-type, eggs from mothers carrying $brk^{KO}$ and $brk^{3M}$ follicle cell clones have (A) only one reduced or no DAs ($P < 0.0001$), (B) the opercula are significantly larger ($P < 0.0001$) and (C) the micropyle are significantly reduced ($P < 0.01$). Eggs from $brk^{CM}$ and $brk^{\Delta 3R}$ homozygous mothers have (A) significantly shorter DAs ($n = 10$, $P < 0.0001$), (B) opercula appear wild-type ($n = 10$, $P > 0.05$) and (C) micropyle are reduced ($n = 10$, $P < 0.01$). Eggs from mothers carrying $brk^{\Delta 3RCM}$ follicle cell clones have (A) significantly shorter or no DAs ($P < 0.0001$) occasionally being as severe as $brk^{KO}$, (B) opercula that are significantly expanded ($P < 0.0001$) and (C) reduced micropyle ($P < 0.01$). Eggs from mothers carrying $brk^{GM}$ follicle cell clones have (A) wild-type DAs ($P > 0.05$), (B) slightly expanded opercula ($P < 0.05$) and (C) wild-type micropyle ($P > 0.05$). Eggs from mothers carrying follicle cell clones of the *gro* null allele, $gro^{MB36}$ have (A) shorter DAs compared to wild-type ($n = 10$, $P < 0.01$), (B) wild-type opercula ($n = 10$, $P > 0.05$) and (C) reduced micropyle ($P < 0.01$). P values calculated using the Mann Whitney U test, $n = 20$ unless indicated.

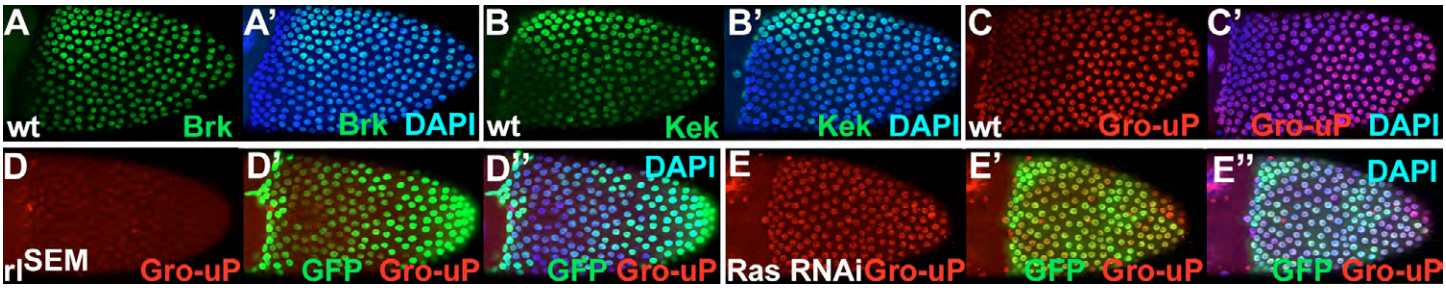


**Fig. S9. Gro phosphorylation by EGFR signaling in the follicular epithelium.** Duplication of egg chambers in Fig. 8, now showing DAPI and UAS-GFP.

**Table S1. Primers used in PCR to generate homology arms and to amplify genomic DNA from mutants**

| Primer | Sequence |
|---|---|
| brkExtF2 | atgcggtaccCAAGTCAAGATGGCTTGC |
| 3SB5PH2 | gatcggtaccTCATAACTCGCGATCTGG |
| brk3PKOF1 | gatccctaggATGCGCCTATACATAGAG |
| brk3PKOR2 | gatccctaggGTGTTCGTGTCAATGTGTGC |
| brkres5P2 | gatcCAGCATTTTGATATAAATTTATC |
| attRrev2 | gatcGTTACCCCAGTTGGGGCACTAC |
| wneo3F3 | CTGTTTATTGCCCCCTCAAA |
| brkres3P1 | gatcCGCGTGCGTGTATATTTATG |
| 5brkfor2 | gatcGTGCCAGTGTGTGTATGTG |
| brkres5P1 | gatcGAATGCTCAAGAGACGTG |
| brkwrev1 | gatcGAGGGAGAGTCACAAAACG |
| brkAmpF2 | gatcCTGGTGAGTACTCAACCAAG |
| 3Pbrkrev1 | gatcGTATAGGCGCATTCCTAGGC |
| attLfor1 | gatcCTCTCAGTTGGGGGCGTAG |
| brk3PR3 | GCCCTATGTTTTGCCCAGT |
| 5brkfor1 | gatcCACAACTATATAGATTTGAAAC |
| loxPR3 | GAAGTTATGGTACCTTAATATTTC |

See Fig. S2 for location of primers.